

# SAGAN-II : Molecular gas content of Giant Radio Galaxies <sup>\*</sup>

P. Dabhade<sup>1,2\*\*</sup>, F. Combes<sup>3,4</sup>, P. Salomé<sup>3</sup>, J. Bagchi<sup>2</sup>, and M. Mahato<sup>2</sup>

<sup>1</sup> Leiden Observatory, Leiden University, P.O. Box 9513, NL-2300 RA, Leiden, The Netherlands

<sup>2</sup> Inter-University Centre for Astronomy and Astrophysics (IUCAA), Pune 411007, India

<sup>3</sup> Sorbonne Université, Observatoire de Paris, Université PSL, CNRS, LERMA, 75014 Paris, France

<sup>4</sup> Collège de France, 11 Place Marcelin Berthelot, 75231 Paris, France

Received 2020/ Accepted 2020

## ABSTRACT

Radio galaxies with jets of relativistic particles usually are hosted by massive elliptical galaxies with active nuclei powered by accretion of interstellar matter onto a supermassive black hole (SMBH). In some rare cases (<5%) their jets drive the overall structure to sizes larger than 700 kpc, and they are called Giant Radio Galaxies (GRGs). A very small fraction of the population of such radio galaxies contains molecular and atomic gas in the form of rings or disks that can fuel star formation. The origin of this gas is not well known, sometimes associated to a minor merger with a gas-rich disk galaxy (e.g. Centaurus A) or cooling of material from a hot X-ray atmosphere (e.g. cooling flows). The giant radio jets might be the extreme evolution of these objects, and they can teach us about the radio galaxy evolution. We have selected 12 targets from a catalogue of 820 GRGs, susceptible to be in a gas accretion and star formation phase. The targets were selected from mid-infrared to contain heated dust. We report here the results of IRAM-30m observations, the molecular gas content, the efficiency of star formation, and discuss the origin of gas and disk morphology. Most of our targets belong to the main sequence (MS), and a large fraction are in the passive domain. Their star formation efficiency is comparable to normal galaxies, except for two of them deficient in molecular gas with a short ( $\sim 200$  Myr) depletion time, and a quiescent gas-rich giant spiral galaxy. In general, the depletion time is much larger than the giant radio jet's life-time.

**Key words.** Galaxies: active — Galaxies: ISM — Galaxies: jets — Galaxies: nuclei — Galaxies: spiral — Radio continuum: galaxies

## 1. Introduction

In recent times it has become evident that a 'co-evolution' (Heckman & Best 2014) exists between galaxies and their central supermassive black holes (SMBH), and new research continues to bring forth new facts, improving our understanding. The simultaneous growth of SMBH and bulges of galaxies could be a consequence of AGN feedback playing a fundamental regulating role on star formation (SF), and could result in the observed tight correlation between their masses (e.g., Croton et al. 2006; Magorrian et al. 1998; Marconi & Hunt 2003). Energy transfer from the AGN can produce outflows and temporarily starve galaxies from fresh gas, thus quenching the star formation (e.g., Ciccone et al. 2014). Therefore, it is now understood that the galaxy's SMBH can play a vital role in its growth and evolution and vice-versa. Most spectacular manifestations of massive black holes in AGNs are the powerful bipolar relativistic jets, that produce twin-lobed structures on  $\sim 10^2$ - $10^3$  kpc scales. Most of the time, evidence for SF quenching is obtained from studying radio-loud AGN, where molecular gas is entrained by the radio jets. These radio galaxies (RGs) are a unique opportunity to study the AGN-fueling process during the radio-mode phase as well as the AGN feedback.

The AGN feedback and outflows can be studied via cold molecular gas properties of the galaxy, and current studies

have been restricted to mostly luminous AGNs. In the past three decades several studies at lower (Evans et al. 2005; Ocaña Flaquer et al. 2010; Prandoni et al. 2010; Smolčić & Riechers 2011; Salomé et al. 2015; Lanz et al. 2016; Ruffa et al. 2019) and higher redshifts (Hughes et al. 1997; van Ojik et al. 1997; De Breuck et al. 2003; Emonts et al. 2014; Nesvadba et al. 2017) have been conducted to probe the molecular gas content, SFR and cold gas as potential fuel supply in RGs. A CO study of a sample of low luminosity RGs carried out by Prandoni et al. (2010) supports the idea that RGs may possible be fuelled by cold gas, restricted to kpc-scale nuclear disks or rings around the AGN. Ruffa et al. (2019) have shown a strong possibility of jet-cold gas interaction in a few objects and inflows inferred from dominant radial motions indicating cold gas fueling the RGs.

An extreme sub-class of RGs, which grows to mega-parsec scales and is relatively rare, is called the Giant Radio Galaxy (GRG). The projected linear size of GRGs is greater than 0.7 Mpc and can grow up to about 5 Mpc, which is comparable to one of the largest galaxy clusters. This makes them one of the largest single astrophysical objects known to us. They have accreting SMBHs of mass  $10^8 - 10^{10} M_{\odot}$ , which under certain conditions launch collimated, bipolar relativistic jets orthogonal to their accretion disk (Lynden-Bell 1969; Begelman et al. 1979). Like normal radio galaxies, GRGs are almost always hosted by bright elliptical galaxies.

<sup>\*</sup> Based on observations carried out with IRAM-30m

<sup>\*\*</sup> E-mail: pratik@strw.leidenuniv.nl

GRGs were discovered (Willis et al. 1974) almost 20 years after the discovery of RGs (Jennison & Das Gupta 1953), and since then only about 820 (Dabhade et al. 2020a) of them have been found, compared to thousands of RGs. The large scale radio properties of GRGs have been extensively studied (Subrahmanyan et al. 1996; Ishwara-Chandra & Saikia 1999; Schoenmakers et al. 2001; Machalski et al. 2001; Konar et al. 2004; Saripalli et al. 2005; Jamrozy et al. 2008; Dabhade et al. 2020b) but AGN and host galaxies have not been studied in great details until now. Therefore, the question of why only certain RGs - the GRGs grow to megaparsec scales is open and needs to be addressed. The study of birth, growth, evolution and duty cycle of GRGs using multi-wavelength approach can perhaps provide important clues to understanding the radio-loudness of AGNs, which constitute less than 20% of the entire AGN population known. Other problems related to GRGs and their interpretation models have been discussed in Dabhade et al. (2020a).

Some CO observations of GRGs have been attempted before (3C236: Labiano et al. 2013, 3C 326: Nesvadba et al. 2010) but were mostly single object studies. Saripalli & Mack (2007), as part of their work on restarted RGs, observed 5 GRGs with the 15m Swedish-ESO Millimetre Telescope (SEST) in the CO(1-0) and CO(2-1) line transitions and obtained only upper limits for all their GRGs.

To understand these extreme cosmic radio sources better, and specifically address the key questions about their size and power, we have initiated a project called SAGAN<sup>1</sup> (Search and Analysis of GRGs with Associated Nuclei), whose pilot study was presented in Dabhade et al. (2017). Under this project, we have built a uniform database of all known GRGs which did not exist before (Dabhade et al. 2020a). With this GRG database, we aim to carry out multi-wavelength studies of their host galaxies, focusing on physical properties such as their black hole accretion rate, their excitation type:– either high-power radiatively-efficient giant radio galaxies ("high-excitation", HEGRG), or low-power radiatively-inefficient radio galaxies ("low-excitation", LEGRG), the black hole mass ( $M_{\text{BH}}$ ), their galaxy star formation rate (SFR), their molecular gas content. The key to understanding the giant nature of GRGs may lie in the accretion properties of these peculiar AGNs, and we can probe these by tracing molecular gas to find whether these objects are fueled from cold gas in the disk. The presence or absence of cold molecular gas in the host galaxies of GRGs can provide information about their star formation rate, accretion state, and stellar mass properties.

The rest of the paper is organised in the following way: In Section. 2, we describe our sample; observations are presented in Section. 3, and the results in Section. 4. The interpretation of these results, and their impact in the evolution scenarios are discussed in Section. 5. The conclusions of our work are presented in Section. 6. To compute distances, we adopt a flat  $\Lambda$ CDM cosmology, with  $\Omega_{\text{m}}=0.29$ ,  $\Omega_{\Lambda}=0.71$ , and the Hubble constant  $H_0 = 70 \text{ km s}^{-1}\text{Mpc}^{-1}$ .

## 2. The sample

Under project SAGAN (Dabhade et al. 2020a), we have created the largest database of GRGs to date, and we applied the following criteria to form a sub-sample to be studied at

millimetre waves using IRAM to probe the cold molecular gas content:– (i) the GRG is not hosted by a quasar, (ii) the GRG is well detected in the Wide-field Infrared Survey Explorer (WISE) at  $22\mu\text{m}$  (4<sup>th</sup> band) (Wright et al. 2010), (iii) the redshift of the host galaxy of the GRG is accurately known via spectroscopic measurements, (iv) the GRG is observable in the sky of IRAM-30m telescope. After applying all the above filters on our GRG-catalogue, we selected a sample of 12 GRGs, which is listed in Table. 1. In column 3 and 4 of Table. 1, we have listed the accurate position (RA & Dec) of the host galaxies, and their accurate spectroscopic redshifts are in column 5. Column 6 includes the luminosity distances of the sources. The information obtained from the WISE 4<sup>th</sup> band and its derived properties are presented in subsequent columns 7 & 8, wherein column 8,  $L_{22\mu\text{m}}$  is the luminosity of the host galaxies at  $22\mu\text{m}$ . Column 9 contains the GRG references of the sources, and/or the optical identification. Figure. 1 displays the SDSS images for those sources when they are available. For the others, the PanSTARRS i band images of the hosts of the GRGs in our sample are given in Figure. 2.

For all the 12 galaxies of the sample, the star formation rate (SFR) was first estimated from the  $22\mu\text{m}$  luminosity (Calzetti et al. 2007). When a more accurate estimation existed in the literature from the SED, or multi-wavelength tracers, we used it from Chang et al. (2015) for R1-2, R1-3, R2-0, R2-3, R2-6 to R2-9, and from Salim et al. (2018) for R2-0, R2-3, R2-7 and R2-8. As several estimations are available, we take an average value. Stellar masses were estimated from observed optical and near infrared (NIR) magnitudes, using standard relations as a function of colours, derived from stellar populations models (Bell et al. 2003). Since the targets have a small redshift, K-corrections have been applied, using the analytical approximations from Chilingarian et al. (2010). All adopted values are listed in Table. 2, together with our CO results obtained using IRAM-30m data. Table. 2 also lists the angular sizes (column 2) of the galaxies, acquired from NED which can be compared from Figures. 1 and 2.

### 2.1. R1-1: 2MASX J23453268–0449256

The galaxy 2MASX J23453268–0449256 (R1-1) is one of the largest (projected linear size  $\sim 1.6$  Mpc at radio wavelengths) radio galaxy known until now, hosted by a massive, late-type spiral galaxy lacking a classical bulge at the redshift of 0.0755 (Bagchi et al. 2014). It shows FR-II and ‘double-double’ (two sets of lobes indicating episodic activity) radio morphology, with the jet axis being nearly orthogonal to the host galaxy’s disk. This is very unusual since such large scale radio jets are in general hosted by ellipticals (Taylor et al. 1996; McLure et al. 2004). It shows several other unusual properties which challenge the standard paradigms for black hole growth in galaxies lacking classical bulges. Its general properties as presented by Bagchi et al. (2014) and Bagchi et al. (2020 - in preparation) are similar to those of passive red spirals (Masters et al. 2010), although the WISE mid-IR colours suggest that star formation is still occurring within its disk. With  $M_r \sim -23.0$  mag, it lies at the very top of the luminosity function of red spirals. The galaxy’s rotation curve peaks at about  $429 \pm 30 \text{ km s}^{-1}$  at large radius which is quite high among all spirals, after correcting for  $i = 65^\circ$  inclination angle (cf

<sup>1</sup> <https://sites.google.com/site/anantasakyatta/sagan>

Table 1: General properties of our sample of 12 GRGs is presented in this table. Here R1 and R2 refers to observation run 1 and 2 respectively with IRAM-30m. RA and Dec are expressed in J2000 coordinate system. Object R1-0 is a radio loud quasar, and object R2-0 is a radio galaxy. Both these objects were recently classified as non-GRGs based on new available data. All the redshifts listed column 5 are from spectroscopic measurements, where redshifts marked with † sign are from SDSS. In the absence of SDSS spectroscopic redshift measurement, the redshift was taken from the reporting paper (Column 9) .

Sr.No	Name	RA	Dec	$z$	$D_L$	W4 (22 $\mu$ m)	Log $L_{22\mu\text{m}}$	Ref
(1)	(2)	(HMS)	(DMS)	(5)	(Mpc)	mag (snr)	(erg s <sup>-1</sup> )	(9)
(1)	(2)	(3)	(4)	(5)	(6)	(6)	(8)	(9)
R1-1	2MASX J23453268–0449256	23 45 32.70	–04 49 25.4	0.07557	342	7.135 (8.5)	43.35	(1)
R1-2	CGCG 245–031	13 12 17.00	+44 50 21.3	0.03557 <sup>†</sup>	156	8.133 (5.7)	42.27	(2)
R1-3	B2 1029+28	10 32 14.02	+27 56 01.7	0.08519 <sup>†</sup>	389	6.821 (11)	43.58	(2)
R2-1	WNB0313+683	03 18 18.98	+68 29 31.4	0.09010	412	6.187 (23.9)	43.18	(3)
R2-2	LCRS B132559.3–025215	13 28 34.37	–03 07 44.8	0.08526 <sup>†</sup>	389	7.067 (13.5)	42.77	(4)
R2-3	2MASX J14504940+1006497	14 50 49.40	+10 06 49.1	0.05453 <sup>†</sup>	243	8.112 (4.9)	41.95	(5)
R2-4	NGC 6251	16 32 31.97	+82 32 16.4	0.02471	108	5.561 (33)	42.24	(6)
R2-5	LEDA 2785926	21 45 30.90	+81 54 53.7	0.14570	692	6.320 (28.3)	43.57	(7)
R2-6	B2 0951+27	09 54 19.19	+27 15 59.9	0.47120 <sup>†</sup>	2649	7.469 (7.0)	44.26	(8,9)
R2-7	LEDA 1406818	10 21 24.21	+12 17 05.4	0.12940 <sup>†</sup>	606	8.248 (3.5)	42.66	(10)
R2-8	Specs	14 09 48.85	–03 02 32.5	0.13749 <sup>†</sup>	651	8.332 (2.2)	42.69	(11)
R2-9	J121615.21+162432.1	12 16 15.21	+16 24 32.2	0.45908 <sup>†</sup>	2569	7.556 (6.3)	44.19	(12)
R1-0	PKS 0211–031	02 13 47.00	–02 56 37.5	0.35679	1906	7.412 (8.8)	44.73	(13)
R2-0	B2 0915+32B (NE)	09 18 59.41	+31 51 40.7	0.06212	278	8.582 (3.3)	41.85	(14)

– References (1) Bagchi et al. (2014) – (2) Schoenmakers et al. (2001) – (3) Schoenmakers et al. (1998) – (4) Machalski et al. (2001) – (5) Clarke et al. (2017) – (6) Waggett et al. (1977) – (7) Schoenmakers et al. (2000) – (8) Proctor (2016) – (9) Amirkhanyan (2016) – (10) Koziel-Wierzbowska & Stasińska (2011) – (11) Hota et al. (2011) – (12) Dabhade et al. (2020a) – (13) Owen et al. (1995) – (14) Kuźmicz et al. (2018).

Hyperleda<sup>2</sup>). This implies an estimated dynamical mass of  $\sim 10^{13} M_{\odot}$  within the virial radius of 450 kpc, assuming a flat rotation curve. The central bulge velocity dispersion is  $\sigma = 351 \pm 25 \text{ km s}^{-1}$ , close to the highest velocity dispersion found among nearby E and S0 galaxies (van den Bosch et al. 2012). Walker et al. (2015) used Chandra to detect the galaxy’s hot X-ray halo, which extends to  $r > 80 \text{ kpc}$ ; it is one of just a few high-mass spirals for which hot gaseous halos have been directly detected via X-ray imaging to date (Bregman et al. 2018). Intriguingly, the X-ray emitting hot halo is highly elongated parallel to the host galaxy disk, suggesting that feedback by the radio jet has disrupted or expelled hot gas from a region extending roughly 80 kpc above and below the disk plane. Such a radio mode feedback is rarely seen in spiral galaxies (Mukherjee et al. 2016, 2018).

## 2.2. R1-2: CGCG 245–031

CGCG 245–031 (R1-2) is a flat-spectrum radio source (Healey et al. 2007). Having a low value for its absolute spectral index, it is a young radio source, a good candidate for a restarting class.

## 2.3. R1-3: B2 1029+28

B2 1029+28 is hosted by a Seyfert type 1 galaxy (Véron-Cetty & Véron 2006) called 2MASX J10321402+2756015

<sup>2</sup> <http://leda.univ-lyon1.fr/>

in which the stellar populations are not old but have intermediate ages (Kuźmicz et al. 2019).

## 2.4. R2-1: WNB0313+683

The GRG R2-1 or WNB0313+683 has a projected linear size of 1.52 Mpc with a GPS (GHz-peaked spectrum) core, FR-II type morphology and recurrent activity (Schoenmakers et al. 1998; Bruni et al. 2019). It is hosted by a Seyfert type-1 galaxy (LEDA 3095635) at  $z \sim 0.09$  which is detected in hard X-rays (Winter et al. 2008). Schoenmakers et al. (1998) estimated its spectral age to be  $\sim 144 \text{ Myr}$ , however, recently Machalski (2011) estimated the lobes’ age to be  $\sim 250 \text{ Myr}$ .

## 2.5. R2-2: LCRS B132559.3–025215

Machalski & Condon (1999) identified LCRS B132559.3–025215 as a GRG, which is hosted by a Seyfert 2 (Véron-Cetty & Véron 2006) type of galaxy called 2MASX J13283434–0307442.

## 2.6. R2-3: 2MASX J14504940+1006497

Source R2-3 is hosted by central dominant galaxy (the core of a triplet, which is also known as UGC 09555 NED03) of a low-density galaxy group (MSPM 02158), as seen in Figure. 1. Clarke et al. (2017), based on their SED analysis, concluded the host galaxy to be a S0-type galaxy with

SFR of  $1.2 \pm 0.3 M_{\odot} \text{ yr}^{-1}$ . Clarke et al. (2017) also present its LoFAR 142 MHz radio map which reveals a large angular diffuse structure, not seen in any other radio survey. The presence of bright radio core and large diffuse emission along the jet axis strongly indicates a restarted source. Based on its radio core spectrum it has been classified as a flat-spectrum (Healey et al. 2007) between  $\sim 1$  to 10 GHz frequencies and has an inverted core spectrum between 22 to 43 GHz frequencies (Park et al. 2013). This further supports the restarted AGN scenario.

## 2.7. R2-4: NGC 6251

NGC 6251 is our nearest target, and has been the object of many observations, since its identification (Waggett et al. 1977; Laing et al. 1983). Chen et al. (2011) studied the neighboring 17 galaxies, which may form a loose group, but with very low background X-ray gas, explaining the large 1.6 Mpc radio jets. The main jet and lobes are centre-brightened like an FR-I, but there are also hot spots near the end of the north and south lobes suggestive of an FR-II. The radio power is in between the two FR types. Recent LOFAR observations at 150 MHz have revealed low surface brightness extensions and backflows of the lobes (Cantwell et al. 2020), with ages larger than 200 Myr. A dust lane has been discovered by Nieto et al. (1983), roughly parallel to the radio jet, with a size about 5 kpc. The inner orientation of the jets is still unclear, at least it appears that there is some misalignment between the inner jet and outer lobes (Jones & Wehrle 2002).

## 2.8. R2-8: Speca

Only about  $\sim 10$  RGs (Ledlow et al. 2001; Hota et al. 2011; Bagchi et al. 2014; Singh et al. 2015; Mao et al. 2015; Mulcahy et al. 2016) have been found to be hosted by spiral galaxies up to now, and only two (2MASX J23453268–0449256 and Speca) of them belong to the GRG subclass. Along with its unusual property of being hosted by a spiral (Hota et al. 2011), Speca is also the Brightest Galaxy (BCG) of a WHL J140948.9-030232 (also called MaxBCG J212.45357-03.04237) cluster. Another peculiar property of this object is its three pairs of lobes, also called as triple-double with clear evidence of restarting activity. The outer lobes look like relics revived by shocks coming from the interaction between the cluster and cosmic filaments. The galaxy shows very recent star formation ( $\sim 500$  Myr), which could be fueled by a cooling flow (Hota et al. 2011).

## 2.9. Other GRGs

R2-5 (Seyfert 2) and R2-7 are also dominant galaxies of their groups, with indices of star formation in a recent past (Kuźmicz et al. 2019). R2-9 is one of the most recently identified GRG, at relatively high redshift (Dabhade et al. 2020a), which appears to be actively forming stars. R2-9 is the most luminous GRGs at 22 microns (WISE band 4) in our sample and appears to be harbouring a dust obscured powerful AGN based on its red colour.

## 2.10. Non-GRGs

B2 0915+32B is a galaxy pair, the two companions being at 43 kpc distance. The northern galaxy of early-type is the host of the giant radio jet, and its southern companion is a late-type blue spiral galaxy, which could be the reservoir of gas to fuel the northern AGN. PKS 0211-031 is radio loud quasar with FR-II type morphology.

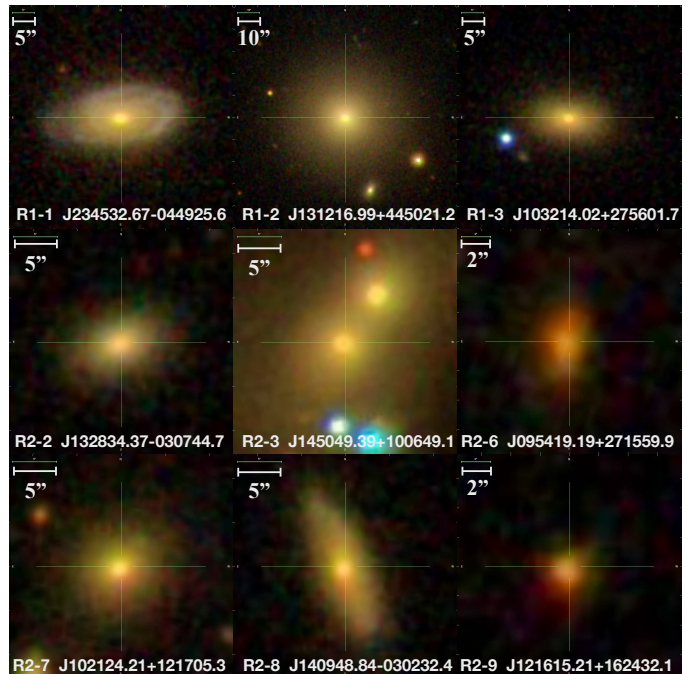


Fig. 1: Host galaxies of 9 GRGs from SDSS. The bar on top left represents the angular scale in arcseconds for reference.

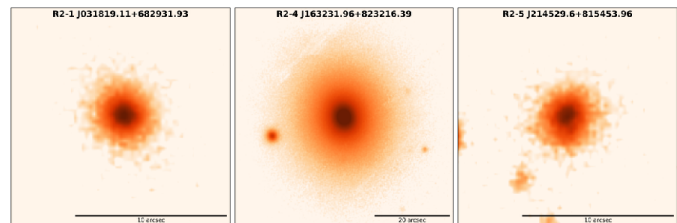


Fig. 2: PanSTARRS *i* band image of the hosts of GRGs, absent in the SDSS footprint. The bar at bottom indicates the angular scale of 5'', 20'' and 10'' respectively, for R2-1, R2-4, and R2-5.

## 3. Observations

Observations of the CO(1-0), CO(2-1) (and for one target CO(3-2)) emission lines have been carried out with the IRAM-30m telescope at Pico Veleta, Granada, Spain, during June and September 2016 for the first run (called R1), and then in March 2020 for the second run (called R2). The beam full width at half-maximum (FWHM) is 23'' and 12'' at the frequencies of 115 GHz and 230 GHz, respectively. Our targets (except two) have redshifts ranging from 0 to 0.1, and the corresponding beams are up to 10% larger, accordingly. The SIS receivers (EMIR) were used for observations

in the wobbler-switching mode, with reference positions offset by  $\pm 120$  arcsec in azimuth. The main-beam efficiency of IRAM is  $\eta_{\text{mb}} = T_{\text{A}}^*/T_{\text{mb}} = 0.79$  and  $0.63$  at  $105$  GHz and  $210$  GHz, respectively. The system temperatures ranged between  $150$  K and  $400$  K at  $2.6$  mm and between  $200$  K and  $600$  K at  $1.3$  mm. The pointing was regularly checked every 2 hours on a nearby planet or a bright continuum source, and the focus was reviewed after each sunrise or if a suitable planet was available, as well as at the beginning of each day. The time on source typically ranged from 4 to 5 hours according to the weather. Two backends were used simultaneously, the autocorrelator WILMA (Wideband Line Multiple Autocorrelator) and the FTS (the Fourier transform spectrometer). The  $T_{\text{mb}}$  rms noise level in 4 hours integration was  $\sigma_{\text{mb}} \sim 0.7$  mK with a spectrometer resolution of  $50 \text{ km s}^{-1}$  for  $105$  GHz and  $\sigma_{\text{mb}} \sim 0.9$  mK for  $210$  GHz. These can be lower in very good weather. The upper limits reported in next section for the integrated CO fluxes are computed by  $S(\text{CO})dV = 3 \times \text{rms}_{300} \text{ JypK} \times 300 \text{ km s}^{-1}$  where  $\text{JypK}$  is the conversion from K to Jy ( $=5 \text{ Jy K}^{-1}$  for the IRAM-30m) and  $\text{rms}_{300}$  is the rms estimated in  $300 \text{ km s}^{-1}$  wide bins.

Two of our sample sources were already observed with the IRAM-30m by [Ocaña Flaquer et al. \(2010\)](#). For NGC 6251, we combine our spectra in CO(1-0) to improve the upper limit and provide a CO(2-1) search which was absent. As for B2 0951+32B, which is a pair of galaxies distant by  $36''$ , the previous pointing was directed towards the NED middle position in between the two galaxies, and not covering any. We observed towards the north-eastern elliptical galaxy, which is the host of the RG ([Fanti et al. 1987](#)).

#### 4. Results

As shown in Table. 2, only the spiral galaxy R1-1 (J2345–0449) has been clearly detected, and upper limits are reported for the 11 other GRGs, with tentative detections for two of them. The two-horn spectra of R1-1 (Figure. 3) have been fitted by 3 gaussians each, and the fits are reported in Table. 3. These fits are only empirical, which is better for computing the total intensity, but do not imply any underlying physical components. Note that the upper limit for the R1-0 RG (PKS0211–031) is relatively high, since it is one of the highest redshift sources. However, the molecular mass is expected to increase with redshift ([Tacconi et al. 2018](#)), and with the measured SFR, a much higher molecular mass was expected. Therefore, the upper limit is significant. The tentative signals are displayed in Figure 4 for CO(2-1) in the spiral galaxy Specca, and CO(1-0) for J121615.21+162432.1. Only linear baselines have been subtracted from the spectra, however, uncertainties are present due to wavy baselines, although the signal appears at  $5\sigma$  and  $6\sigma$  respectively.

In the following subsections, we present our results derived from our detections and upper limits of the molecular gas content of the hosts of GRGs, and also compare it with the SFR derived from the mid-IR fluxes. Using our observed quantities we were also able to estimate the gas depletion time  $t_{\text{dep}} = M(\text{H}_2)/\text{SFR}$  and compare it with the radiative lifetime of the GRGs. From the shape of the detected profile (two-horn shape, and contrast), we derive the gas concentration in the host and discuss the origin of the cool gas. The two-horn profile indicates the presence of an extended disk or ring suggesting a merger origin for the gas. When

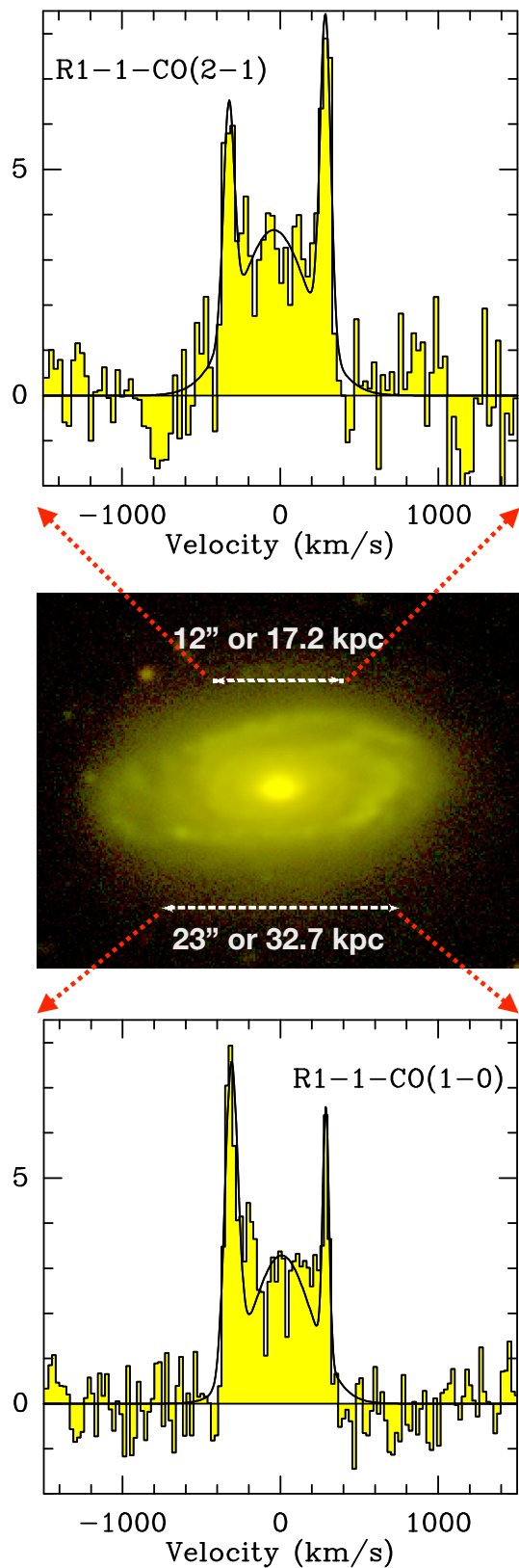


Fig. 3: The two spectra obtained towards R1-1 or GRG-J2345–0449 in CO(1-0) (bottom) and CO(2-1) (top). The vertical scale is  $T_{\text{mb}}$  in mK. The middle optical image of the host spiral galaxy of J2345–0449 is obtained by combining G and R band data of MegaCam on the CFHT. Both G and R band data belongs to the first generation filters on the MegaCam. The scale on the image represents the beam of the IRAM observation at respective frequencies.

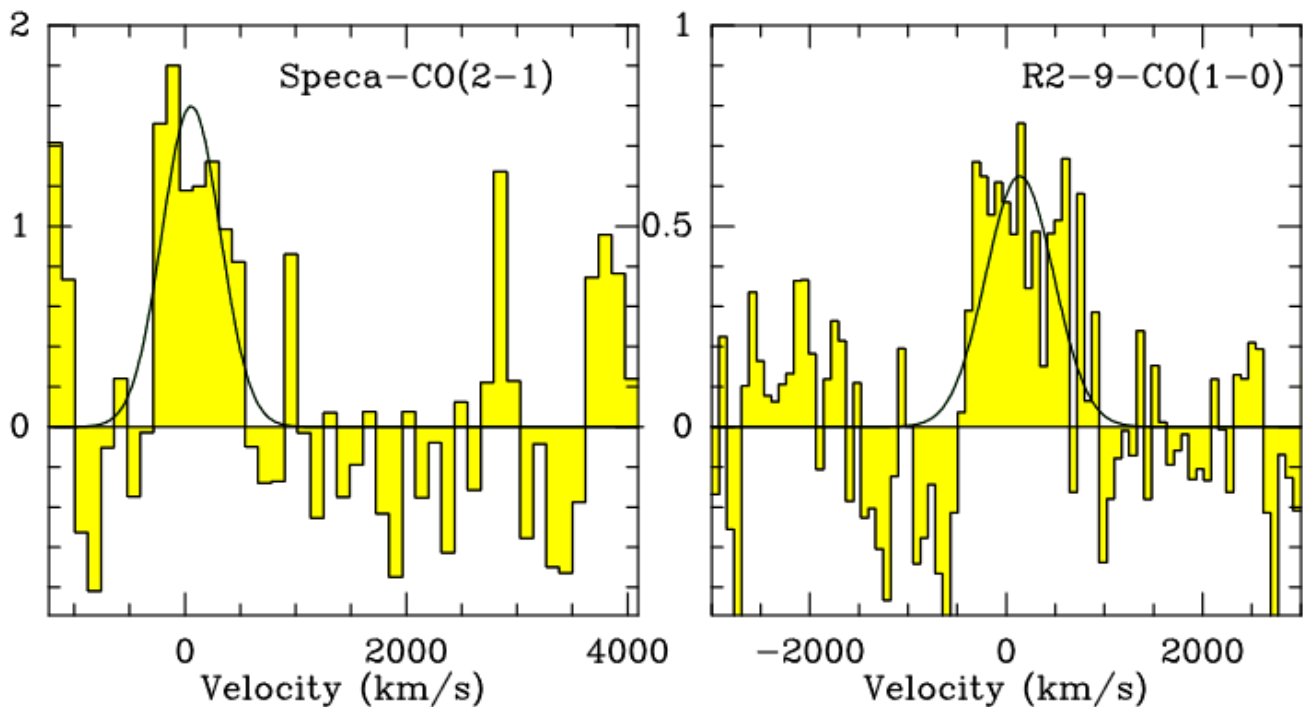


Fig. 4: Tentative spectra obtained towards Speca in CO(2-1) (left) and R2-9 in CO(1-0) (right). The vertical scale is  $T_{\text{mb}}$  in mK.

the gas is just coming from cooling filaments, it generally has no time to relax in the galaxy potential, and such a profile is not expected.

#### 4.1. Molecular masses

To quantify the amount of molecular gas found in each target, we rely on the empirically established proportionality between the CO(1-0) luminosity and  $\text{H}_2$  mass for a large number of Milky Way-like galaxies (e.g., Bolatto et al. 2013). We converted the integrated intensities in each beam (in  $T_{\text{mb}}$ ) into integrated fluxes  $S(\text{CO})dV$ , with the conversion of 5 Jy per Kelvin, as appropriate for the IRAM-30m telescope. From the integrated CO(1-0) flux  $S(\text{CO})dV$  ( $\text{Jy km s}^{-1}$ ) found within each region, the molecular mass was obtained through the formula (e.g., Solomon & Vanden Bout 2005):

$$L'_{\text{CO}}(\text{K km s}^{-1}\text{pc}^{-2}) = 3.25 \times 10^7 \frac{S(\text{CO})dV}{(1+z)} \left( \frac{D_L}{\nu_{\text{rest}}} \right)^2$$

where  $\nu_{\text{rest}} = 115.271$  GHz, and  $D_L$  is the luminosity distance in megaparsec. The molecular mass, including helium, was then derived from  $M(\text{H}_2) = 4.36 L'_{\text{CO}}$  assuming the standard CO-to- $\text{H}_2$  conversion factor of  $X_{\text{CO}} = 2 \cdot 10^{20} \text{ cm}^{-2} (\text{K km s}^{-1})^{-1}$ , as applicable to Milky Way-like galaxies.

The region encompassed by the CO(1-0) beams in each galaxy is sufficiently large to cover all the CO emission (even in the nearest one, NGC 6251 (R2-4), it is 11 kpc). It is, therefore, possible to compare the total molecular masses with other published samples without any aperture correction.

#### 4.2. Deconvolving the two-horn spectra

In Figure 3, the CO(1-0) and CO(2-1) spectra show a two-horn shape, with a different depth between the two peaks, with the CO(1-0) spectrum being deeper. This means that the molecular component is not too highly concentrated towards the centre, and that we are beginning to resolve it in the CO(2-1) line. To interpret more quantitatively the kinematics of our CO data, we use a simple analytical model which computes the velocity spectrum from the rotation velocity profile of the galaxy (Wiklind et al. 1997). The rotation velocity profile is determined from the stellar mass distribution, assuming it follows the simple potential-density pair, proposed by Hernquist (1990). We adjust the size and mass of the stellar component to fit the half-light radius and  $M_*$  shown in Table 2. We complete this mass at high radii by dark matter, in order to flatten the rotation curve. The dark matter mass inside 24.5 kpc is taken to be  $1.5 M_*$ , and its characteristic radius is 3 times that of the stars. The gas disk is also taken into account in the potential, as shown in Figure 5, with the mass shown in Table 2. Its characteristic scale can be determined through the two-horn spectra modelling. Based on the ellipticity obtained from the optical image (Figure 1), we derive an inclination of  $65^\circ$ , which is also close to the value given by Hyperleada ( $65.7^\circ$ ).

The gas distribution is assumed to be axisymmetric of surface density  $\Sigma(r)$  in a disc with negligible thickness. For each velocity  $dv$ , the code calculates the density contained in the isovelocity (equation 1). The velocity spectrum corresponds to the histogram of the velocities. We then convolve the computed spectrum with a gaussian of standard

Table 2: Derived properties of the GRG sample where  $R_e$  is the half-light radius, SFR is the star formation rate, CO refers to CO flux in respective bands,  $\log M(\text{H}_2)$  represents molecular mass (log scale),  $t_{\text{dep}}$  is the deletion time, and  $\log M_*$  refers to the stellar mass (log scale) of the galaxy.

Sr.No	$R_e$ (arcsec)	$R_e$ (kpc)	SFR ( $M_\odot \text{ yr}^{-1}$ )	CO(1-0) ( $\text{Jy km s}^{-1}$ )	CO(2-1) ( $\text{Jy km s}^{-1}$ )	$\log M(\text{H}_2)$ ( $M_\odot$ )	$t_{\text{dep}}$ Gyr	$\log M_*$ ( $M_\odot$ )
(1)	(2)	(3)	(4)	(5)	(6)	(6)	(8)	(9)
R1-1	5.4	7.76	2.95	14.0	16.3	10.21	5.49	11.37
R1-2	6.1	4.32	0.19	<1.7	<2.7	<8.63	<2.24	10.51
R1-3	3.6	5.77	2.45	<1.5	<7.5	<9.35	<0.91	10.84
R2-1	0.96	1.62	2.07	<1.3	<2.2	<9.34	<1.05	10.63
R2-2	2.2	3.53	0.91	<0.9	<1.3	<9.13	<1.48	10.52
R2-3	0.78	0.83	0.09	<0.9	<1.9	<8.73	<5.96	11.25
R2-4 <sup>(2)</sup>	15.6	7.78	0.31	<1.2	<4	<8.16	<0.47	11.40
R2-5	0.7	1.79	4.64	<1.1	<1.9	<9.69	<1.06	11.03
R2-6 <sup>(1)</sup>	0.95	5.63	170	<1.3	<2.7	<10.82	<0.39	11.70
R2-7	2.4	5.59	1.44	<1.1	<1.9	<9.59	<2.70	11.41
R2-8	3.3	8.04	1.48	<0.9	1.1	9.04	0.74	11.50
R2-9 <sup>(1)</sup>	0.6	3.55	8.33	0.54	<1.1	10.42	3.15	10.89
R1-0 <sup>(1)</sup>	0.87	4.37	48.9	<0.45	<1.6	<10.11	<0.26	10.87
R2-0	5.6	6.70	0.47	<1.1	<2.7	<8.93	<1.81	11.46

– (1) For these sources, we observed CO(3-2) instead of CO(2-1) – (2) This source was also observed by [Ocaña Flaquer et al. \(2010\)](#) – All upper limits are computed at  $3\sigma$  and assuming FWHM =  $300 \text{ km s}^{-1}$ .

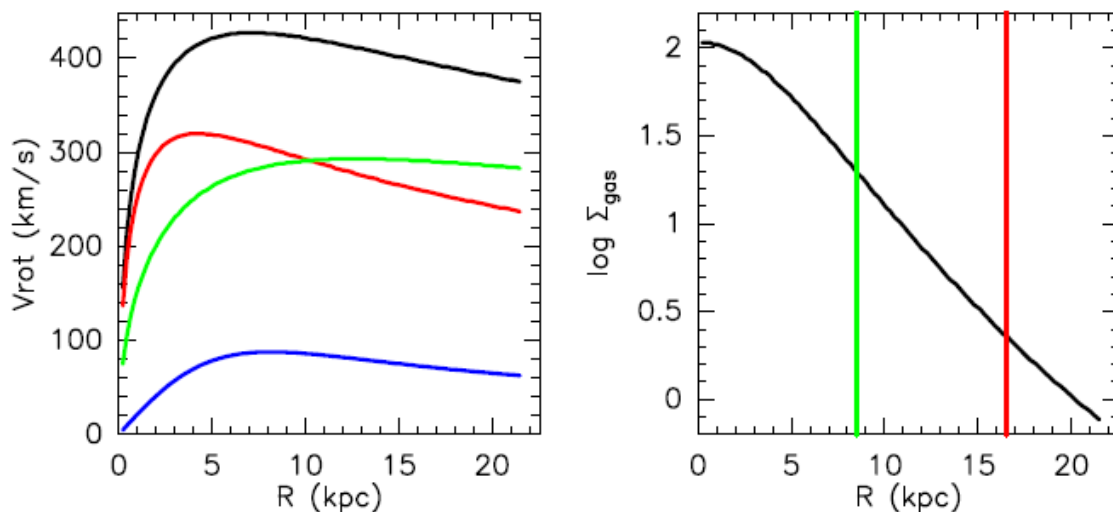


Fig. 5: The mass model for R1-1 or GRG-J2345–0449 is shown at left, with the contributions to the rotational velocity of the stellar mass (red), the dark matter (green) and the gas (blue). The right panel shows the adopted gas surface density, with the two vertical lines indicating the FWHM beam of the CO(1-0) (red) and CO(2-1) (green).

$\sigma = 10 \text{ km s}^{-1}$ , to account for the gas velocity dispersion.

$$\frac{dN}{dv}(v) = \int \frac{\Sigma(r) r dr}{v_{\text{rot}}(r) \sin i \left(1 - \left[\frac{v}{v_{\text{rot}}(r) \sin i}\right]^2\right)^{1/2}} \quad (1)$$

To determine the concentration of gas in the galaxy, we adopt an analytical profile, with a potential-density pair, which makes the computation of the rotation velocity easy. We select the formulation of a Toomre disc of order 2:  $\Sigma(r) = \Sigma_0 \left(1 + \frac{r^2}{a^2}\right)^{-5/2}$  (Toomre 1964). As can be seen in Figure. 5, the profile is close to an exponential, which is

realistic. We also tried models with rings, using the difference between two Toomre disks with different scales, but a single gas disk was even a better fit. The exponential scale of the best fit disk is 4.34 kpc, leading to a half-light radius of 7.3 kpc, very close to that of the stellar component. This corresponds to what is generally found for the molecular distributions (Lisenfeld et al. 2011).

## 5. Discussion

GRGs are quite rare when compared to the RG population, and very few studies have been conducted to detect molecular gas in their host galaxies. We have tabulated the detec-

Table 3: Fit results for R1-1 (GRG-J2345–0449) CO spectra.

Line	Area <sup>(1)</sup> mK km s <sup>-1</sup>	V km s <sup>-1</sup>	FWHM km s <sup>-1</sup>	T <sub>mb</sub> peak mK
CO(1-0)	1232±167	-316±4	207±11	5.6±0.8
CO(1-0)	800±121	10±18	235±50	3.2±0.8
CO(1-0)	779±150	291±15	179±30	4.1±0.8
CO(2-1)	930±115	-324±8	141±20	6.2±0.9
CO(2-1)	1368±265	-35±33	357±70	3.6±0.9
CO(2-1)	972±110	286±5	113±13	8.1±0.9

– (1) Integrated signal in main beam temperature scale

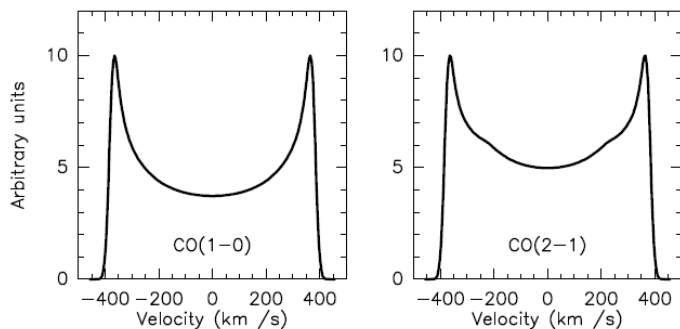


Fig. 6: The spectra obtained from the model, for the CO(1-0) line with a beam of  $23'' = 33$  kpc (left) and for the CO(2-1) line with a beam of  $12'' = 17$  kpc (right). The assumed inclination of the disk is  $65^\circ$ .

Table 4: Molecular gas in other GRGs from literature

Name	R <sub>e</sub> kpc	SFR M <sub>⊙</sub> yr <sup>-1</sup>	log M(H <sub>2</sub> ) M <sub>⊙</sub>	log M <sub>*</sub> M <sub>⊙</sub>	Ref
NGC315	6.3	0.63	7.87	11.49	(1)
3C31	4.6	1.02	9.22	11.29	(1)
3C236	7.4	7.51	9.32	11.15	(2)
3C326N	6.9	0.67	9.18	11.40	(3)

– (1) Ocaña Flaquer et al. (2010); (2) Labiano et al. (2013); (3) Nesvadba et al. (2010)

tions reported in the literature in Table. 4. In the following section, we consider all the four GRGs listed in Table. 4 hosted by early-type galaxies. NGC 315 is the brightest elliptical (cD) galaxy of a group (O’Sullivan et al. 2015), and has been also detected in HI-21cm absorption and emission (Morganti et al. 2009). 3C 31 hosted by NGC 383 is a lenticular galaxy which is well detected in CO (Evans et al. 2005; Ocaña Flaquer et al. 2010), but neither in emission nor in absorption (Emonts et al. 2010) of HI-21cm. The host of 3C 236 is a massive elliptical galaxy, with distorted morphology, and a prominent dust lane. Its CO spectrum is blue-shifted by  $\sim 300$  km s<sup>-1</sup> with respect to the optical velocity (Labiano et al. 2013), and corresponds to the peak of the HI-21cm absorption (Morganti et al. 2005). The maximum and minimum spectral ages of different parts of GRG 3C 236 is 159 Myr and 51 Myr respectively (Shulevski et al. 2019). The radio core of 3C 326 comprises of two early-type galaxies, with the most massive one in the North (3C 326N

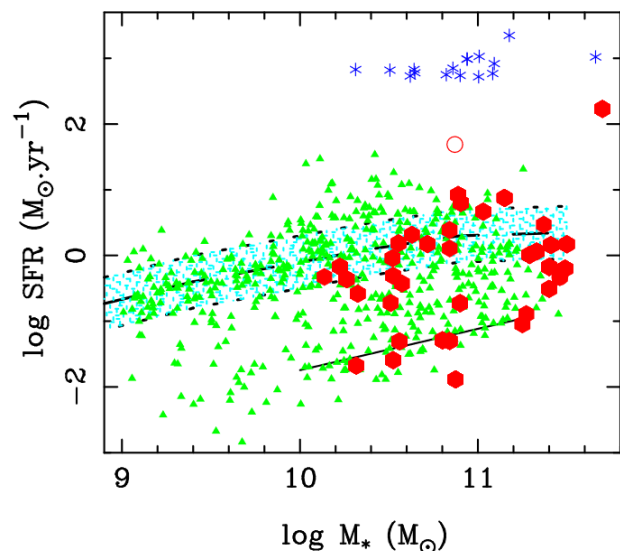


Fig. 7: Location of our targets (red hexagons) in the SFR- $M_{\text{star}}$  diagram. They are compared with the xCOLD GASS sample of 532 galaxies, with local redshift  $0.01 < z < 0.05$ , from Saintonge et al. (2017) (green triangles), and with the starburst galaxies (blue stars) in the comparable range  $0.2 < z < 0.6$  (Combes et al. 2011). The SDSS main sequence is materialized by a cyan-shaded region, and delimited by dashed lines (at  $\pm 0.4$  dex), and the red sequence by a full line. Open red circles belong to non-GRGs observed by us.

: 15:52:09.10 +20:05:48.32) being the host galaxy (Rawlings et al. 1990). Its molecular gas is in both cold phase (Nesvadba et al. 2010) and warm phase (Ogle et al. 2007) tracing shocks, possibly due to the radio jets feedback.

### 5.1. Star formation and gas mass

The host galaxies of GRGs have not previously been studied with respect to their SFR as a function of stellar mass and compared with the main sequence galaxies, starbursts or quiescent objects. We have attempted to do so as seen in Figure. 7, where we have selected the xCOLD GASS sample of Saintonge et al. (2017) as a reference to trace the main sequence at low redshift and as part of the red sequence. Starburst galaxies at comparable redshifts are plotted from Combes et al. (2011). It is important to have samples at the same  $z$ , since the location of the main sequence depends strongly on redshift (Whitaker et al. 2012). Eight of our targets are in the main sequence (MS), including the detected R1-1, while four are in a starburst phase, and seven are in the red passive sequence. The position close to the MS is associated with disk morphology (Wuyts et al. 2011), while the slope and scatter of the MS depends on morphology (Whitaker et al. 2015).

The star formation rate is expected to be related to the interstellar gas content, and the precise relationship has been discussed either from the atomic or molecular gas or both (Kennicutt 1998; Bigiel et al. 2008). The relation is much tighter and linear with the molecular gas. The relation can be expressed with the global quantities (SFR versus  $M_{\text{mol}}$ ), or with the surface densities, when normalised with the effective area. The latter are computed from the effective radius, containing half of the light (displayed in Table.



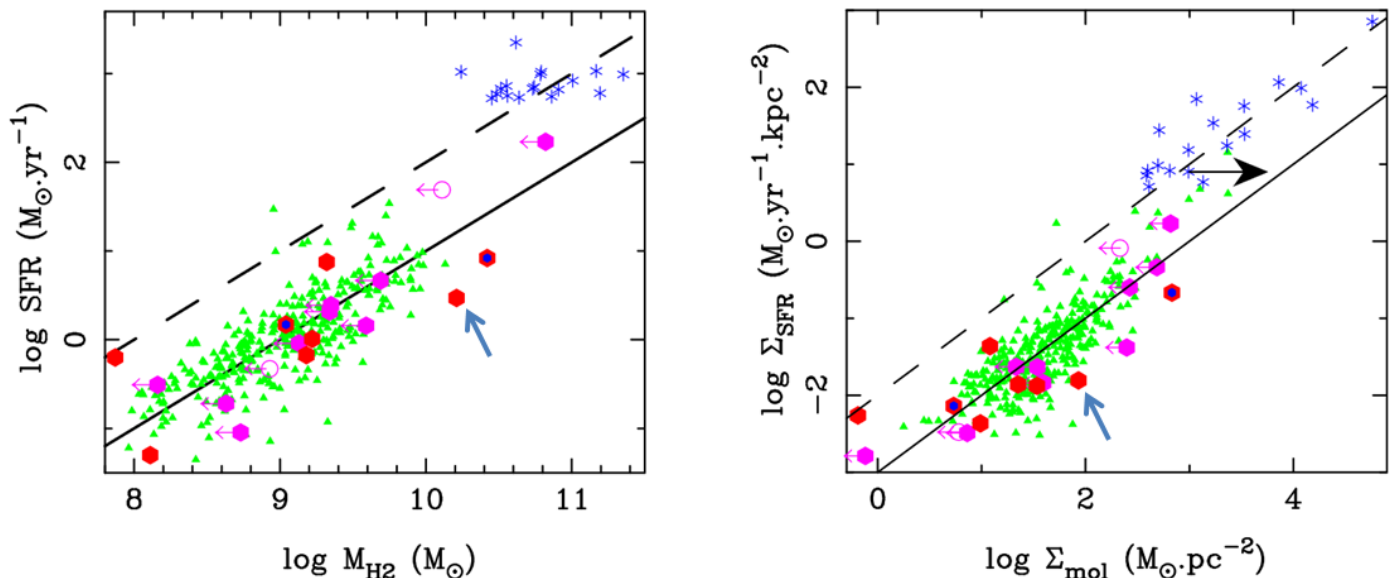


Fig. 8: The star formation rate SFR as a function of the molecular content, for our targets compared to normal galaxies and starbursts at comparable redshifts. Left is the global SFR- $M_{\text{mol}}$  diagram, and right the surface densities of the same quantities, representing the unresolved Kennicutt-Schmidt (KS) relation (Kennicutt 1998). The straight lines drawn are power-laws of slope 1. The full line corresponds to a depletion time of 1 Gyr and the dashed line 100 Myr. Symbols are like in Figure. 7, with now upper limits of our targets in pink, and tentative detections with a blue hexagon inside the red one. The blue arrow points to the location of R1-1 (GRG-J2345–0449) on the respective plots.

2). This is a global quantity for the galaxy since we do not resolve the inner parts of the galaxies with our observations with IRAM-30m. Figure. 8 displays both relations. In the global quantities diagram, most of our upper limits fall in the region of normal MS galaxies, traced by the straight line corresponding to a depletion time  $t_{\text{dep}} = M(\text{H}_2)/\text{SFR} = 1$  Gyr. The R1-1 detected spiral galaxy has a large  $t_{\text{dep}}$  of 5.5 Gyr, as well as the tentative detection R2-9 ( $t_{\text{dep}}$  of 3.15 Gyr) while two detected GRG (NGC 315 and 3C 236) have exceptionally short  $t_{\text{dep}}$  of 120 and 280 Myr, as well as two upper limits, more typical of starbursts. When normalised to the galaxy surface, the R1-1 spiral galaxy and other outliers fall much closer to the main sequence in the KS diagram, except for NGC 315 and NGC 6251, which are still exceptionally deficient in molecular gas. R1-1 which is a giant spiral galaxy, despite having a large reservoir of  $M_{\text{H}_2}$  does not have high SFR as seen in Figure. 8, which may have a connection with the restarted nature of the GRG. Note that in these relations, the molecular masses of the starburst sample have been obtained with a different CO-to- $\text{H}_2$  conversion factor, as justified for starbursts (Solomon & Vanden Bout 2005). With a larger factor, the difference with the MS would be much smaller, as indicated by the arrow in the right panel of Figure. 8.

The fraction of gas among the baryonic content of a galaxy, measured by the gas to stellar mass ratio, is a key factor in understanding the various star formation rates observed. This relative gas content is plotted versus the specific SFR (sSFR= $\text{SFR}/M_*$ ) as seen in the left plot in Figure. 9. The GRG targets follow the main sequence galaxies of the xCOLD GASS sample, with two of them being gas poor, NGC 315 and NGC 6251. Together with the gas fraction, SFR depends on the efficiency of star formation with respect to the amount of fuel, i.e.  $\text{SFR}/M_{\text{mol}}$ , which is the inverse of the depletion time  $t_{\text{dep}}$ . The latter is plotted ver-

sus sSFR in Figure. 9 right. Here again, most of our targets follow the MS scaling relations, except two of them, appearing too efficient to form stars, because of lack of molecular gas.

Table 5: Other properties of GRGs. We have computed  $P_{1.4}$ , D and  $Q_{\text{Jet}}$  from the data available in the literature - the 6<sup>th</sup> column indicates whether the GRG shows signs of restarted AGN activity, and their belonging to a group (Gr) or cluster (Cl).

Sr	FR type	$\log P_{1.4}$ W Hz <sup>-1</sup>	D Mpc	HE/LE	Restart Gr/Cl	$Q_{\text{Jet}}$ ( $10^{43}$ erg s <sup>-1</sup> )
R1-1	II	24.31	1.64	LE	Yes	-
R1-2	I	23.95	0.96	LE	Gr	-
R1-3	II	24.71	1.05	HE	Gr	0.53
R2-1	II	25.20	1.52	HE	Yes	2.45
R2-2	II	24.57	1.47	HE	Gr	-
R2-3	I/II	-	2.48	LE	Gr	0.36
R2-4	I/II	24.41	1.96	SF	No	1.21
R2-5	II	25.36	2.80	HE	Gr	1.77
R2-6	II	25.94	1.79	HE	No	17.94
R2-7	II	24.71	2.24	LE	Gr	-
R2-8	II	24.83	1.39	LE	Yes	-
R2-9	II	26.02	1.78	HE	No	16.53
NGC 315	I/II	24.15	1.15	SF	Gr	0.16
3C 31	I	24.48	0.93	LE	Gr	0.54
3C 236	II	26.05	4.45	HE	Yes	14.76
3C 326N	II	25.66	2.02	LE	Yes	10.42

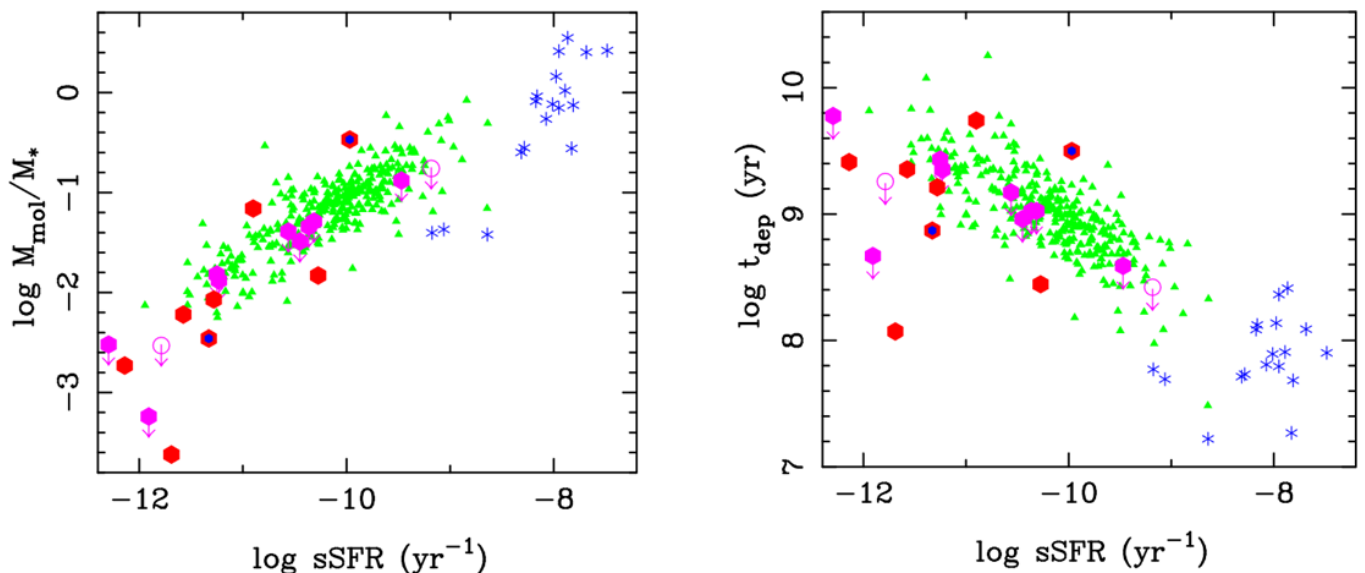


Fig. 9: As a function of specific star formation rate sSFR, the molecular gas to stellar mass ratio (left) and the depletion time (right). Symbols are like in Figure. 8.

### 5.2. Radio power and fueling

The nuclear activity in galaxies is thought to be triggered when the central supermassive black hole accretes a significant mass of gas, from its interstellar reservoir. Typical accretion phases in AGN may last  $\sim 40$  Million years, with a duty cycle of a few percent (Shankar et al. 2009; Hopkins & Quataert 2010). The GRGs are thought to be at the end of an active and powerful phase of radio galaxy evolution. Several hypotheses have been proposed to account for their extreme sizes, but the role of each factor is still unclear. Among possibilities there is the power of the radio jet, implying a larger velocity (Schoenmakers et al. 2000), the influence of the environment (jets being able to extend more in voids, however see Dabhade et al. 2020a), or a restarted activity (Bruni et al. 2019, 2020). In the latter case, the sources are identified with two jets at different orientations, called double-double, or X-shaped (Saripalli et al. 2013), and/or a young central source (Machalski et al. 2007), with a flat spectral index (Schoenmakers et al. 1998), which has recently been refueled.

The determination of their gas reservoir can confirm and quantify these fueling mechanisms, and help to understand the complex processes involved in their radio jet launching and evolution. The important clues for the giant nature of GRGs may lie in the accretion rates, which translate in terms of high excitation (HE) or low excitation (LE). The HE objects are defined to have an accretion rate above one hundredth of the Eddington rate, while the LE objects accrete below. The latter belong to a regime of radiatively inefficient accretion, which are fostering the formation of radio jets. Table. 5 indicates the excitation character of the source (HE/LE) or star formation (SF) character. Dabhade et al. (2020a) have established that GRGs do not preferentially have high or low excitation type AGN and have a mixed population of both, which is similar to that of RG population. The distribution of their black mass is also similar to that of RGs. Having ruled out the above factors for the giant nature of GRGs, it is imperative to look at other processes in the galaxies which are contrasting to the RGs.

As seen in Table. 2, we have classified GRGs in our sample with respect to their AGN excitation type- high and low or HEGRG and LEGRG. We find that HEGRGs tend to have higher molecular gas mass compared to LEGRGs, and this is consistent with the findings of Smolčić & Riechers (2011), who find a similar trend for RGs. In Dabhade et al. (2020a), we have shown that LEGRGs and HEGRGs show distinct properties like their respective low sized counterparts LERGs and HERGs. Here, we have shown that, the distinction in their properties extends even to molecular gas content as well.

Recent gas accretion could be violent, through major mergers, or more secular via minor mergers of cold gas accretion from cosmic filaments. The observation of the molecular component may bring important clues, showing a perturbed component in case of galaxy interaction, or a regular disk for secular evolution. It has been observed that the detection rate of molecular gas is high in the edge darkened Fanaroff-Riley (FR) type 1 radio galaxy (Fanaroff & Riley 1974) and low in edge brightened FR-II type (Evans et al. 2005). More than 90% of the GRGs have FR-II type of morphology (Dabhade et al. 2020c,a) and it is very interesting to check if GRGs with FR-II type morphology too have less molecular gas detection.

Table. 5 summarizes the FR type, total radio power ( $P_{1.4}$ ), projected linear size (D), excitation state, and jet kinetic power ( $Q_{\text{Jet}}$ ) of all GRGs in our sample along with other GRGs taken from literature. The 1.4 GHz power was estimated using the NRAO VLA Sky Survey (Condon et al. 1998) flux of the GRG at 1.4 GHz. We use the method given by Hardcastle (2018) to estimate  $Q_{\text{Jet}}$  using the 150 MHz flux from TIFR GMRT Sky Survey (Intema et al. 2017) and other observations from the literature. A similar scheme was used in Dabhade et al. (2020a) to compute the above parameters for a large sample of GRGs. The excitation status (accretion mode) of GRGs is determined from the mid-infrared fluxes, as in Dabhade et al. (2020a). It helps separate star-forming from AGN dominated emitting objects, as well as high excitation (HE) from low excitation

(LE) radio galaxies with the mid-infrared ratios obtained in the WISE bands. WISE colours have been demonstrated to be very useful diagnostics of the accretion mode of radio galaxies (Gürkan et al. 2014).

Evans et al. (2005) conducted a survey to investigate the molecular content in RGs, where they found detections in FR-I and compact sources, but rarely in FR-II objects. It could be expected that restarted RGs, requiring molecular gas to fuel their activity, would be detected, but only a few have been found to be rich in molecular gas, among them the post-merger 3C293 (Ocaña Flaquer et al. 2010; Labiano et al. 2014). Evans et al. (2005) also checked for a possible correlation between the CO luminosity and the 1.4 GHz core luminosity and found none. We studied the possible effect of the radio jets on the host galaxies' properties via exploring connections between  $Q_{\text{Jet}}$  and parameters derived from our IRAM-30m observations. Based on the current data, we do not find any correlation between the above mentioned parameters. The above results may not be uncovering the whole aspect as our observations with IRAM-30m presents the global cumulative molecular gas properties, and correlations may exist for nuclear region components only.

Our clear CO detection involves a giant spiral galaxy (R1-1), and one tentative signal comes from the spiral Spca (R2-8). All other detections are from early-type galaxies, but with dust lanes in the centre. Radio jets and in particular giant ones are rare in spiral galaxies, which may have several explanations. The origin could come from the energetic power of the central engine, since the black hole mass is proportional to the spheroidal stellar mass (e.g., Kormendy & Ho 2013). In addition, the radio jets are launched around black holes with a significant spin (Blandford & Znajek 1977), and black holes in elliptical galaxies acquire the largest spins, due to major mergers (Fanidakis et al. 2011). But also, one factor is precisely the existence of giant molecular clouds (GMC) in spiral galaxies, which provide obstacles to a young radio jet, may bend its direction and make it unstable (Wang et al. 2000).

The giant size of radio jets can be due to the combined effect of the energy of the central engine (the jet power), the duration of its activity, and the effect of environment, in particular, how fast is the density of the intergalactic medium decreasing with radius. Self-similar studies (Falle 1991; Kaiser et al. 1997) have succeeded to model the observed Power-Size (P-D) diagrams, through evolutionary tracks. They model the energy-losses in the radio cocoon, including the re-accelerations in the hot spots. Important selection effects have to be taken into accounts, in particular the youth-redshift degeneracy (Blundell et al. 1999). These different works have come to an average model of a powerful radio source, where the luminosity first increases with time until 10 Myr, and then decreases, while the size of the radio lobes increases to the giant values, until  $\sim 100$  Myr (Blundell & Rawlings 1999). The Malmquist bias then explains why high-redshift sources appear in general younger (around 10 Myr).

GRGs have a larger amount of intermediate age stellar populations compared with smaller sized FR-II radio sources (Kuźmicz et al. 2019). This is also true for their neighbours within 1.5 Mpc, which show in general younger populations, suggesting triggered star formation due to their environment. This triggering, either through mergers or cold streams, might also be responsible for their giant

sizes. A large fraction of GRGs in our sample belong to groups, like R1-2, R1-3, R2-2, R2-3, R2-5 and R2-7 (cf Table. 5). The R2-3 in, particular, resides at the centre of a quite disturbed tight galaxy group. It is one of the galaxies of the UGC9555 triplet, hosting a compact flat-spectrum radio source (Clarke et al. 2017). There is evidence that the AGN has been fueled by recent interactions and minor mergers from its group galaxies. None of the other galaxies in the sample show any signs of recent mergers, that could be responsible for their fueling.

Finally, most of the CO-detected GRGs belong to the restarted class, implying that the molecular gas has recently (within  $\sim 100$  Myr) refuelled the AGN and radio jets. However, there seems to be a competition between star formation and nuclear activity for the fueling. Among these galaxies, some are actively forming stars and their depletion time is quite short (740 Myr and 280 Myr for Spca and 3C236 respectively), while others are rather quiescent and favouring the AGN, like R1-1 and 3C326 (with  $t_{\text{dep}}$  of 5.5 Gyr and 2.26 Gyr). Using observations of Hubble Space Telescope, Tremblay et al. (2010) have shown bursts of repeated star formation in the host galaxy of 3C 236, which has dusty disc around the AGN. Since 3C 236 is known to be restarted AGN, there could be a connection with the young starburst property of the host galaxy. Based on the studies of GRGs conducted so far and our results, we understand that we are observing each GRG in its different evolutionary phase. Therefore, we are unlikely to find a similar fueling trend (e.g cold gas fueling) for all GRGs, since it is closely dependent on the AGN accretion state.

In the future, it will be fruitful to observe the GRGs with ALMA to probe the sphere of influence of its black holes residing in the AGN. This will possibly be a test for the presence of a molecular torus as recently found in some low luminosity AGNs by Combes et al. (2019).

## 6. Summary

We have presented our first IRAM results for a sample of 12 GRGs, selected from the GRG-catalogue (Dabhade et al. 2020a). We have detected the two first rotational lines of CO in one GRG, which is a giant spiral GRG-J2345–0449, and report tentative signals for two others (R2-8 and R2-9). The two-horn shape of the spectra allowed us to determine the concentration of the molecular gas in the giant spiral galaxy. The best fit model is a roughly exponential disk for the molecular component, with a half-light radius comparable to that of the stellar component.

We added 4 GRGs from the literature with CO lines detections to our sample. Comparing this sample of 16 GRGs with the main-sequence (MS) star-forming galaxies at comparable redshift from Saintonge et al. (2017) and a sample of starburst galaxies at similar  $z$  (Combes et al. 2011), we find that most (8) of our targets are in the MS, while seven are in the red sequence and four are starbursts. The molecular content of our targets is quite compatible with what is expected from their star formation rate (SFR), although our detected giant spiral appears to be deficient in star formation, with a depletion time of 5.5 Gyr, about 3 times longer than the average of the MS.

Most of our molecular gas detected galaxies belong to the restarted radio galaxies, or are in groups, suggesting that the environment plays an important role to refuel the central AGN. The accreted gas also fuels star formation,

and the depletion time is sometimes quite short, a few 100 Myr, i.e. comparable to time-scales similar to spectral ages of the GRGs. Up to now, the number GRGs with CO detections is not high, and more detections should be obtained to draw firmer conclusions.

*Acknowledgements.* This work is based on observations carried out with the IRAM 30m telescope. IRAM is supported by INSU/CNRS (France), MPG (Germany) and IGN (Spain). PD, FC and JB gratefully acknowledge generous support from the Indo-French centre for the Promotion of Advanced Research (Centre Franco-Indien pour la Promotion de la Recherche Avancée) under programme no. 5204-2. JB, PD and MM would like to thank IUCAA Radio Physics Laboratory and the facilities therein for their support. PD acknowledges the support of Leiden University. This publication has made use of data products from the NASA/IPAC Extragalactic Database (NED). We acknowledge the usage of the HyperLeda database (<http://leda.univ-lyon1.fr>). The IRAM staff at Pico Veleta are gratefully acknowledged for their help with the 30m observations. This work was supported by the Programme National Cosmology et Galaxies (PNCG) of CNRS/INSU with INP and IN2P3, co-funded by CEA and CNES.

## References

- Amirkhanyan, V. R. 2016, *Astrophysical Bulletin*, 71, 384
- Bagchi, J., Vivek, M., Vikram, V., et al. 2014, *ApJ*, 788, 174
- Begelman, M. C., Rees, M. J., & Blandford, R. D. 1979, *Nature*, 279, 770
- Bell, E. F., McIntosh, D. H., Katz, N., & Weinberg, M. D. 2003, *ApJS*, 149, 289
- Bigiel, F., Leroy, A., Walter, F., et al. 2008, *AJ*, 136, 2846
- Blandford, R. D. & Znajek, R. L. 1977, *MNRAS*, 179, 433
- Blundell, K. M. & Rawlings, S. 1999, *Nature*, 399, 330
- Blundell, K. M., Rawlings, S., & Willott, C. J. 1999, *AJ*, 117, 677
- Bolatto, A. D., Wolfire, M., & Leroy, A. K. 2013, *ARA&A*, 51, 207
- Bregman, J. N., Anderson, M. E., Miller, M. J., et al. 2018, *ApJ*, 862, 3
- Bruni, G., Panessa, F., Bassani, L., et al. 2019, *ApJ*, 875, 88
- Bruni, G., Panessa, F., Bassani, L., et al. 2020, *MNRAS*, 494, 902
- Calzetti, D., Kennicutt, R. C., Engelbracht, C. W., et al. 2007, *ApJ*, 666, 870
- Cantwell, T. M., Bray, J. D., Croston, J. H., et al. 2020, *MNRAS*, 495, 143
- Chang, Y.-Y., van der Wel, A., da Cunha, E., & Rix, H.-W. 2015, *ApJS*, 219, 8
- Chen, R., Peng, B., Strom, R. G., & Wei, J. 2011, *MNRAS*, 412, 2433
- Chilingarian, I. V., Melchior, A.-L., & Zolotukhin, I. Y. 2010, *MNRAS*, 405, 1409
- Cicone, C., Maiolino, R., Sturm, E., et al. 2014, *A&A*, 562, A21
- Clarke, A. O., Heald, G., Jarrett, T., et al. 2017, *A&A*, 601, A25
- Combes, F., García-Burillo, S., Audibert, A., et al. 2019, *A&A*, 623, A79
- Combes, F., García-Burillo, S., Braine, J., et al. 2011, *A&A*, 528, A124
- Condon, J. J., Cotton, W. D., Greisen, E. W., et al. 1998, *AJ*, 115, 1693
- Croton, D. J., Springel, V., White, S. D. M., et al. 2006, *MNRAS*, 365, 11
- Dabhade, P., Gaikwad, M., Bagchi, J., et al. 2017, *MNRAS*, 469, 2886
- Dabhade, P., Mahato, M., Bagchi, J., et al. 2020a, *arXiv e-prints*, [arXiv:2005.03708](https://arxiv.org/abs/2005.03708)
- Dabhade, P., Röttgering, H. J. A., Bagchi, J., et al. 2020b, *A&A*, 635, A5
- Dabhade, P., Röttgering, H. J. A., Bagchi, J., et al. 2020c, *A&A*, 635, A5
- De Breuck, C., Neri, R., & Omont, A. 2003, *New A Rev.*, 47, 285
- Emonts, B. H. C., Morganti, R., Struve, C., et al. 2010, *MNRAS*, 406, 987
- Emonts, B. H. C., Norris, R. P., Feain, I., et al. 2014, *MNRAS*, 438, 2898
- Evans, A. S., Mazzarella, J. M., Surace, J. A., et al. 2005, *ApJS*, 159, 197
- Falle, S. A. E. G. 1991, *MNRAS*, 250, 581
- Fanaroff, B. L. & Riley, J. M. 1974, *MNRAS*, 167, 31P
- Fanidakis, N., Baugh, C. M., Benson, A. J., et al. 2011, *MNRAS*, 410, 53
- Fanti, C., Fanti, R., de Ruiter, H. R., & Parma, P. 1987, *A&AS*, 69, 57
- Gürkan, G., Hardcastle, M. J., & Jarvis, M. J. 2014, *MNRAS*, 438, 1149
- Hardcastle, M. J. 2018, *MNRAS*, 475, 2768
- Healey, S. E., Romani, R. W., Taylor, G. B., et al. 2007, *ApJS*, 171, 61
- Heckman, T. M. & Best, P. N. 2014, *ARA&A*, 52, 589
- Hernquist, L. 1990, *ApJ*, 356, 359
- Hopkins, P. F. & Quataert, E. 2010, *MNRAS*, 407, 1529
- Hota, A., Sirothia, S. K., Ohyama, Y., et al. 2011, *MNRAS*, 417, L36
- Hughes, D. H., Dunlop, J. S., & Rawlings, S. 1997, *MNRAS*, 289, 766
- Intema, H. T., Jagannathan, P., Mooley, K. P., & Frail, D. A. 2017, *A&A*, 598, A78
- Ishwara-Chandra, C. H. & Saikia, D. J. 1999, *MNRAS*, 309, 100
- Jamrozy, M., Konar, C., Machalski, J., & Saikia, D. J. 2008, *MNRAS*, 385, 1286
- Jennison, R. C. & Das Gupta, M. K. 1953, *Nature*, 172, 996
- Jones, D. L. & Wehrle, A. E. 2002, *ApJ*, 580, 114
- Kaiser, C. R., Dennett-Thorpe, J., & Alexander, P. 1997, *MNRAS*, 292, 723
- Kennicutt, Robert C., J. 1998, *ARA&A*, 36, 189
- Konar, C., Saikia, D. J., Ishwara-Chandra, C. H., & Kulkarni, V. K. 2004, *MNRAS*, 355, 845
- Kormendy, J. & Ho, L. C. 2013, *ARA&A*, 51, 511
- Kozieł-Wierzbowska, D. & Stasińska, G. 2011, *MNRAS*, 415, 1013
- Kuźmicz, A., Czerny, B., & Wildy, C. 2019, *A&A*, 624, A91
- Kuźmicz, A., Jamrozy, M., Bronarska, K., Janda-Boczar, K., & Saikia, D. J. 2018, *ApJS*, 238, 9
- Labiano, A., García-Burillo, S., Combes, F., et al. 2014, *A&A*, 564, A128
- Labiano, A., García-Burillo, S., Combes, F., et al. 2013, *A&A*, 549, A58
- Laing, R. A., Riley, J. M., & Longair, M. S. 1983, *MNRAS*, 204, 151
- Lanz, L., Ogle, P. M., Alatalo, K., & Appleton, P. N. 2016, *ApJ*, 826, 29
- Ledlow, M. J., Owen, F. N., Yun, M. S., & Hill, J. M. 2001, *ApJ*, 552, 120
- Lisenfeld, U., Espada, D., Verdes-Montenegro, L., et al. 2011, *A&A*, 534, A102
- Lynden-Bell, D. 1969, *Nature*, 223, 690
- Machalski, J. 2011, *MNRAS*, 413, 2429
- Machalski, J. & Condon, J. J. 1999, *ApJS*, 123, 41
- Machalski, J., Jamrozy, M., & Zola, S. 2001, *A&A*, 371, 445
- Machalski, J., Kozieł-Wierzbowska, D., & Jamrozy, M. 2007, *Acta Astron.*, 57, 227
- Magorrian, J., Tremaine, S., Richstone, D., et al. 1998, *AJ*, 115, 2285
- Mao, M. Y., Owen, F., Duffin, R., et al. 2015, *MNRAS*, 446, 4176
- Marconi, A. & Hunt, L. K. 2003, *ApJ*, 589, L21
- Masters, K. L., Mosleh, M., Romer, A. K., et al. 2010, *MNRAS*, 405, 783
- McLure, R. J., Willott, C. J., Jarvis, M. J., et al. 2004, *MNRAS*, 351, 347
- Morganti, R., Peck, A. B., Oosterloo, T. A., et al. 2009, *A&A*, 505, 559
- Morganti, R., Tadhunter, C. N., & Oosterloo, T. A. 2005, *A&A*, 444, L9
- Mukherjee, D., Bicknell, G. V., Sutherland, R., & Wagner, A. 2016, *MNRAS*, 461, 967
- Mukherjee, D., Bicknell, G. V., Wagner, A. e. Y., Sutherland, R. S., & Silk, J. 2018, *MNRAS*, 479, 5544
- Mulcahy, D. D., Mao, M. Y., Mitsuiishi, I., et al. 2016, *A&A*, 595, L8
- Nesvadba, N. P. H., Boulanger, F., Salomé, P., et al. 2010, *A&A*, 521, A65
- Nesvadba, N. P. H., Drouart, G., De Breuck, C., et al. 2017, *A&A*, 600, A121
- Nieto, J. L., Coupinot, G., Lelievre, G., & Madsen, C. 1983, *MNRAS*, 203, 39P
- Ocaña Flaquer, B., Leon, S., Combes, F., & Lim, J. 2010, *A&A*, 518, A9
- Ogle, P., Antonucci, R., Appleton, P. N., & Whysong, D. 2007, *ApJ*, 668, 699
- O'Sullivan, E., Combes, F., Hamer, S., et al. 2015, *A&A*, 573, A111
- Owen, F. N., Ledlow, M. J., & Keel, W. C. 1995, *AJ*, 109, 14
- Park, S., Sohn, B. W., & Yi, S. K. 2013, *A&A*, 560, A80
- Prandoni, I., Laing, R. A., de Ruiter, H. R., & Parma, P. 2010, *A&A*, 523, A38
- Proctor, D. D. 2016, *ApJS*, 224, 18
- Rawlings, S., Saunders, R., Miller, P., Jones, M. E., & Eales, S. A. 1990, *MNRAS*, 246, 21P
- Ruffa, I., Prandoni, I., Laing, R. A., et al. 2019, *MNRAS*, 484, 4239
- Saintonge, A., Catinella, B., Tacconi, L. J., et al. 2017, *ApJS*, 233, 22

- Salim, S., Boquien, M., & Lee, J. C. 2018, *ApJ*, 859, 11
- Salomé, Q., Salomé, P., & Combes, F. 2015, *A&A*, 574, A34
- Saripalli, L., Hunstead, R. W., Subrahmanyan, R., & Boyce, E. 2005, *AJ*, 130, 896
- Saripalli, L. & Mack, K. H. 2007, *MNRAS*, 376, 1385
- Saripalli, L., Malarecki, J. M., Subrahmanyan, R., Jones, D. H., & Staveley-Smith, L. 2013, *MNRAS*, 436, 690
- Schoenmakers, A. P., de Bruyn, A. G., Röttgering, H. J. A., & van der Laan, H. 2001, *A&A*, 374, 861
- Schoenmakers, A. P., Mack, K. H., de Bruyn, A. G., et al. 2000, *A&AS*, 146, 293
- Schoenmakers, A. P., Mack, K. H., Lara, L., et al. 1998, *A&A*, 336, 455
- Shankar, F., Weinberg, D. H., & Miralda-Escudé, J. 2009, *ApJ*, 690, 20
- Shulevski, A., Barthel, P. D., Morganti, R., et al. 2019, *A&A*, 628, A69
- Singh, V., Ishwara-Chandra, C. H., Sievers, J., et al. 2015, *MNRAS*, 454, 1556
- Smolčić, V. & Riechers, D. A. 2011, *ApJ*, 730, 64
- Solomon, P. M. & Vanden Bout, P. A. 2005, *ARA&A*, 43, 677
- Subrahmanyan, R., Saripalli, L., & Hunstead, R. W. 1996, *MNRAS*, 279, 257
- Tacconi, L. J., Genzel, R., Saintonge, A., et al. 2018, *ApJ*, 853, 179
- Taylor, G. L., Dunlop, J. S., Hughes, D. H., & Robson, E. I. 1996, *MNRAS*, 283, 930
- Toomre, A. 1964, *ApJ*, 139, 1217
- Tremblay, G. R., O’Dea, C. P., Baum, S. A., et al. 2010, *ApJ*, 715, 172
- van den Bosch, R. C. E., Gebhardt, K., Gültekin, K., et al. 2012, *Nature*, 491, 729
- van Ojik, R., Roettgering, H. J. A., van der Werf, P. P., et al. 1997, *A&A*, 321, 389
- Véron-Cetty, M. P. & Véron, P. 2006, *A&A*, 455, 773
- Waggett, P. C., Warner, P. J., & Baldwin, J. E. 1977, *MNRAS*, 181, 465
- Walker, S. A., Bagchi, J., & Fabian, A. C. 2015, *MNRAS*, 449, 3527
- Wang, Z., Wiita, P. J., & Hooda, J. S. 2000, *ApJ*, 534, 201
- Whitaker, K. E., Franx, M., Bezanson, R., et al. 2015, *ApJ*, 811, L12
- Whitaker, K. E., van Dokkum, P. G., Brammer, G., & Franx, M. 2012, *ApJ*, 754, L29
- Wiklind, T., Combes, F., Henkel, C., & Wyrowski, F. 1997, *A&A*, 323, 727
- Willis, A. G., Strom, R. G., & Wilson, A. S. 1974, *Nature*, 250, 625
- Winter, L. M., Mushotzky, R. F., Tueller, J., & Markwardt, C. 2008, *ApJ*, 674, 686
- Wright, E. L., Eisenhardt, P. R. M., Mainzer, A. K., et al. 2010, *AJ*, 140, 1868
- Wuyts, S., Förster Schreiber, N. M., van der Wel, A., et al. 2011, *ApJ*, 742, 96